Trapping of point-contact-generated 29-cm^{-1} phonons in ruby

K. Z. Troost, J. I. Dijkhuis, and H. W. de Wijn
Faculty of Physics and Astronomy, and Debye Research Institute, University of Utrecht, P.O. Box 80000, 3508 TA Utrecht, The Netherlands
(Received 8 August 1990)

Trapping of 29-cm^{-1} phonons by optically excited Cr^{3+} ions in ruby is studied at phonon occupations of up to order unity. The 29-cm^{-1} phonons are supplied by transient excitation of a metallic point contact and subsequent conversion of the injected phonons to resonance. The growth and the decay of the trapped phonon population are markedly non-single-exponential quantities, particularly at higher phonon populations. A quantitative analysis of these effects is made on the basis of phenomenological rate equations of the ion and phonon populations. These equations make explicit allowance for the line shape of the $\bar{E}(^2E)-2\bar{A}(^2E)$ phonon transition as well as for feeding and loss of resonant phonons by mediation of weakly exchange-coupled Cr^{3+} pairs. At the higher phonon occupations, the transition appears to be dynamically broadened by stimulated phonon emission, which reduces the trapping efficiency.

I. INTRODUCTION

Trapping of phonons by resonant centers occurs when the mean free path against scattering is small compared to the dimensions of the scattering volume. Multiple scattering in effect results in a diffusive propagation mode, which causes the phonons to stay longer in the active volume than in the case of ballistic propagation. The first experimental observation of imprisonment of high-frequency phonons was accomplished by Geschwind *et al.*,[1] who observed a bottlenecking of 29-cm^{-1} phonons in ruby (Al_2O_3:Cr^{3+}) as a result of resonant scattering involving the $\bar{E}(^2E)-2\bar{A}(^2E)$ transition of optically excited Cr^{3+}. A more systematic investigation of the trapping of 29-cm^{-1} phonons in ruby was initiated by Renk and Deisenhofer.[2] Since that time, the mechanism underlying the escape of resonant phonons from the optically excited zone has been the subject of many theoretical and experimental studies.[3-6] At very low values of the density N^* of metastable Cr^{3+}, spatial diffusion appears to limit the trapping time.[3,7] At higher N^*, however, a flattening out of the trapping time with N^* is observed, indicating that other processes become dominant.[4,5,8,9]

Now there is substantial experimental evidence that in ruby the escape of 29-cm^{-1} phonons from the optically excited volume is mediated by weakly exchange-coupled optically excited Cr^{3+} pairs.[4-6] To account for this, several models involving such pairs have been proposed.[4,5] As it turned out, a pair model based on one-site inelastic scattering of 29-cm^{-1} phonons[5] is consistent with the experiments for reasonable values of the parameters. In this model, a phonon is assumed lost if a scattering event shifts its frequency so far from resonance that its mean free path exceeds the typical dimension of the excited zone (spectral "wipeout"). Spectral wipeout has in this way been identified as the most effective escape mechanism at the higher N^*. Spectral communication also takes place within the trapped phonon packet, but over such small distances that the phonons remain bottlenecked. In a recent high-spectral-resolution study utilizing fluorescence line narrowing (FLN),[10] the spectral dynamics of trapped 29-cm^{-1} phonons was actually observed, and subsequently reproduced by Monte Carlo simulations of one-site inelastic scattering by optically excited pairs. The actual line shape of the $\bar{E}(^2E)-2\bar{A}(^2E)$ phonon transition in ruby was determined in a separate FLN study.[11]

This paper is concerned with experiments on the dynamics of trapped resonant-phonon populations in ruby up to substantial populations. An active zone of Cr^{3+} is maintained in $\bar{E}(^2E)$ by optical pumping, and thermal phonons are removed by cooling to 1.5 K. Phonons are injected over a broad band by transient excitation of a metallic point contact, which has proved to be an efficient generator of high-frequency phonons.[12] These phonons are subsequently converted to resonant ones by the reverse process of wipeout. Non-single-exponential buildup and decay of the trapped phonon population are then observed, with the degree of nonsingle exponentiality depending on the duration and the intensity of the phonon supply. An analysis in terms of phenomenological rate equations of the $2\bar{A}(^2E)$ and phonon populations is carried out with explicit allowance for the line shape of the $\bar{E}(^2E)-2\bar{A}(^2E)$ transition as well as phonon feeding and loss resulting from one-site inelastic scattering by weakly coupled Cr^{3+} pairs. At elevated phonon occupation numbers ($p\sim 1$), reached with intense pulses of longer duration, phonon trapping turns out to become less effective as a result of stimulated emission of resonant phonons and the associated phonon-induced broadening of the transition.

II. EXPERIMENTS

A sufficient concentration of Cr^{3+} ions is maintained in the metastable $\bar{E}(^2E)$ state by optical excitation to the broad $^4T_1$ and $^4T_2$ bands and the subsequent nonradiative decay ultimately to $\bar{E}(^2E)$ on a ps time scale. Metastable Cr^{3+} not only act as resonant scatterers of 29-cm^{-1} phonons by virtue of strong direct spin-phonon coupling, but at the same time serve as detectors of these phonons via the phonon-induced R_2 luminescence (Fig. 1).[2,13] Under bottlenecking conditions, i.e., the phonon undergoes many scattering events before it is removed, the $2\bar{A}(^2E)$ population, monitored via the R_2 luminescence, is a direct measure of the resonant phonon occupation p. Ignoring, for the moment, the intricacies associated with the line shape, we have

$$p = N_{2\bar{A}}/(N_{\bar{E}} - N_{2\bar{A}}) . \quad (1)$$

Note that Eq. (1) reduces to $p = N_{2\bar{A}}/N^*$ at low p, while $N_{2\bar{A}} \approx N_{\bar{E}}$ for high p.

To eliminate any effects of 29-cm^{-1} phonons that are generated in the decay $2\bar{A}(^2E) \rightarrow \bar{E}(^2E)$ of the optical-pumping cycle, the optical pumping is alternately switched on and off for 1 ms. The laser-on period serves to replenish the $\bar{E}(^2E)$ population against its radiative decay ($\tau_R \approx 4$ ms). After the optically generated phonons have decayed, a train of electrical pulses with 1–10-μs separation is applied to the point contact, and the ensuing R_2 luminescence is detected. Note here that in ruby at liquid-helium temperatures, 29-cm^{-1} phonons can be trapped in an optically excited zone for as long as μs, 3 orders of magnitude longer than the spontaneous direct spin-phonon relaxation time T_d of $2\bar{A}(^2E)$. Recent fluorescence-line-narrowing[11] and accumulated-photon-echo experiments[14] have shown that $T_d = 0.7$ ns.

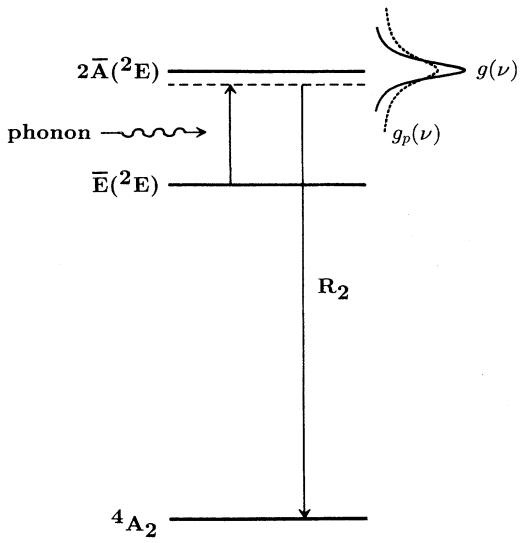

FIG. 1. Phonon detection by Cr^{3+} in ruby. Near-resonant phonons raise metastable Cr^{3+} from $\bar{E}(^2E)$ to $2\bar{A}(^2E)$, resulting in R_2 luminescence. The line shape $g(\nu)$ of the phonon transition broadens with increasing phonon occupation. At 1.5 K, the $\bar{E}(^2E)$ and $2\bar{A}(^2E)$ states are 14 423 and 14 452 cm^{-1} above the $^4A_2$ ground state, respectively.

A Czochralsky-grown ruby crystal, measuring $15 \times 10 \times 7$ mm^3, and with a Cr^{3+} concentration of 700 at. ppm, was used. The c axis was perpendicular to the 15×7-mm^2 faces. A 50-nm-thick metal film, forming the anvil of the point contact, was deposited onto a polished 15×7-mm^2 face by conventional vapor deposition techniques after cleaning with a glow discharge. For good adherence, first a 5-nm thick layer of Cr was deposited, and subsequently, without breaking the vacuum, the Au layer.[15] The spear of the point contact is a 100-μm-diam Au wire, soldered to a 1-mm-diam Ni post serving as a mechanical support. It was electrochemically etched to form a whisker with a tip of approximately 1-μm radius, as determined from electron micrographs. Precise vertical positioning of the whisker against the film under liquid helium was accomplished with a differential screw mechanism operated from outside the cryostat. The point contact was electrically excited using pulses as short as 2 ns with voltages up to 16 V. The impedance of the point contact was monitored via the electrical pulses reflected from the point contact back into the 50-Ω coaxial cable.

The Cr^{3+} centers just below the point contact were optically excited with the beam of an Ar ion laser ($\lambda = 488$ or 514 nm), focused down to a waist of 30 μm with a 50-mm camera lens. The laser beam was directed towards the point contact through the crystal from below, reflecting at an angle of approximately 20° from the film. The luminescence emanating from the detection zone was collected at right angles to the incoming beam, and analyzed with a 0.85-m double monochromator to separate the phonon-induced R_2 luminescence from the much intenser R_1 luminescence. To ensure optical access just below the point contact, the crystal was mounted at an angle of 15° relative to axis of detection. For ballistic phonons traveling at the Debye velocity (≈ 6 km/s), the spatial extent of the detection volume must be 10 μm at most to achieve the desired time resolution of a few ns. This spatial resolution was provided by successive imaging on a horizontal slit and on the vertical entrance slit of the monochromator.

The R_2 luminescence was detected with ns time resolution with standard single-photon counting techniques using a photomultiplier with a rise time of 2.3 ns (RCA C31034). A time-to-amplitude converter, followed by a multichannel analyzer operating in the pulse-height-analysis mode, provided the desired time resolution. When applying pulse sequences with high repetition rates, the start and stop pulses of the time-to-amplitude converter were interchanged to minimize the dead time of the detection system. As already noted, the unwanted R_2 luminescence generated by the optical pumping is removed by limiting the detection to the laser-off period.

III. MODEL

For a quantitative description of the time evolution of the imprisoned 29-cm^{-1} phonon populations coupled with Cr^{3+} in $\bar{E}(^2E)$, we set up phenomenological rate

equations. The equations include, first, escape of imprisoned phonons by spectral wipeout mediated by weakly exchange-coupled pairs consisting of a Cr^{3+} in the optically excited $\bar{E}(^2E)$ state and a Cr^{3+} in the $^4A_2$ ground state. Second, the equations include an explicit treatment of the line shape of the $\bar{E}(^2E)-2\bar{A}(^2E)$ phonon transition in view of its direct relation with the distribution of time constants of the coupled spin-phonon system. Third, the equations account for the pulsed external supply of broadband phonons, which are generated by the point contact and subsequently converted to bottlenecked phonons by the weakly coupled pairs.

To incorporate the effects of weakly coupled Cr^{3+} pairs, we rely on the model developed by Goossens *et al.*[5] This model considers spectral displacements of phonons by inelastic scattering by pairs in a sequence of a spin-nonflip absorption $\bar{E}(^2E)\rightarrow 2\bar{A}(^2E)$ and a spin-flip emission $2\bar{A}(^2E)\rightarrow\bar{E}(^2E)$. The spin-nonflip $\bar{E}(^2E)-2\bar{A}(^2E)$ separation of a Cr^{3+} ion being part of a weakly coupled pair is not notably different from the separation in an isolated Cr^{3+} ion. This was proved with a perturbative calculation,[5] and confirmed later by detailed calculations.[16] The spin-flip transitions of a Cr^{3+} ion in a pair, however, differ in energy by amounts equal to the exchange constant J on either side. The sequence of a spin-nonflip absorption followed by a spin-flip transition back to $\bar{E}(^2E)$ therefore invokes an energy shift $\pm J$ of an incoming resonant 29-cm^{-1} phonon. (J may be chosen positive since no distinction needs to be made between ferromagnetic and antiferromagnetic exchange.) The many long-distance pairs that have small J's obviously do not produce sizable shifts of the phonon energy. However, pairs with a separation of, for instance, 8 Å still have J's of about 0.1 cm^{-1}, and cause displacements far beyond the width of the $\bar{E}(^2E)-2\bar{A}(^2E)$ transition (0.02 cm^{-1} in dilute ruby). These energy shifts are sufficient for the emitted phonon to reach the outer edge of the optically excited zone without being reabsorbed by a weakly coupled Cr^{3+} pair with a matching spin-flip transition, i.e., the phonon has suffered a wipeout.

In the present experiments, the point contact supplies a virtually flat spectrum of phonons. It should be realized, however, that phonons of the central frequency penetrate the excited zone by only a few μm.[10] The point contact, in effect, only maintains a finite phonon occupation throughout the excited zone at energies a few times beyond the linewidth. The Cr^{3+} pairs this time act to convert these phonons to imprisoned ones via the reverse of wipeout, i.e., a spin-flip $\bar{E}(^2E)\rightarrow 2\bar{A}(^2E)$ absorption followed by a spin-nonflip $2\bar{A}(^2E)\rightarrow\bar{E}(^2E)$ emission in a suitable Cr^{3+} pair. We will henceforth refer to this capture of phonons as "wipein."

For tractability of the rate equations, it is useful to divide the excited Cr^{3+} population into two classes according to their effectiveness for wipeout, and, for that matter, wipein (Fig. 2). A criterion for wipeout and wipein may be defined by

$$\Lambda(J)\gtrless L \ , \tag{2}$$

where $\Lambda(J)$ is the mean free path of a phonon shifted from resonance by J, and L is the typical dimension of the optically excited zone. The process relevant for the mean free path is spin-flip absorption, and therefore

$$\Lambda(J)=2\rho v T_d^{(f)}/D(J)N^* \ , \tag{3}$$

where ρ is the density of phonon modes, v is the phonon velocity, $T_d^{(f)}$ is the spontaneous time constant for a spin-flip transition, and N^* is the concentration of excited Cr^{3+} ions. The quantity $D(J)$ is the fraction, per unit of energy, of excited Cr^{3+} that are part of a weakly coupled pair with an exchange splitting J. Accordingly, $\int_0^\infty D(J)dJ=1$. Using the criterion Eq. (2), the two classes are now distinguished according to whether J is smaller (type I) or larger (type II) than a critical exchange J_c defined by $\Lambda(J_c)=L$. Only type-II ions are assumed to invoke a wipeout by a spin-nonflip transition followed by a spin-flip return, and, by the reverse process, to invoke a wipein (Fig. 2). On the other hand, type-I ions are assumed to act as isolated ions. Anticipating the results below, we note that, for parameters typical of the present experiments ($L\sim 200$ μm, $N^*\sim 10^{18}$ cm^{-3} in 700-at. ppm ruby), J_c amounts to 0.022 cm^{-1} according to the expressions given in Ref. 5. Integrating $D(J)$ over all $J>J_c$, we then find $f=0.11$ for the fraction f of excited Cr^{3+} ions classified as type II.

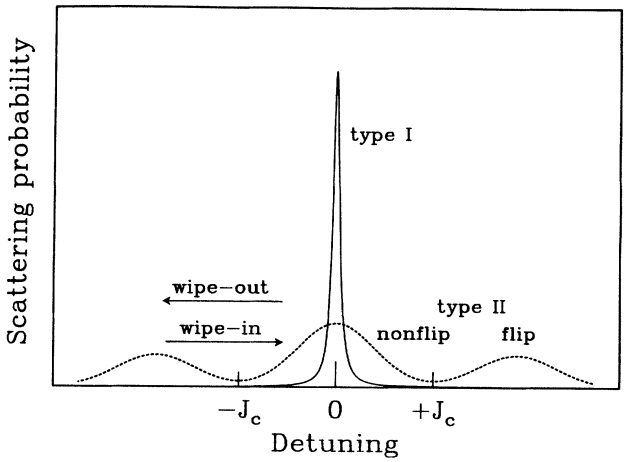

FIG. 2. Schematic diagram of frequency shifs of near-resonant phonons out of resonance (wipeout) and towards resonance (wipein) by mediation of excited type-II Cr^{3+} ions forming part of exchange-coupled pairs. The phonon transition of type-II Cr^{3+} ions is broadened with respect to unperturbed type-I Cr^{3+}.

An effective way of incorporating the line shape of the $\bar{E}(^2E)-2\bar{A}(^2E)$ phonon transition is to make the occupation p and the upper-state population $N_{2\bar{A}}$ dependent on the frequency.[17] The relevant part of the rate equations then takes on the form, in an obvious notation,

$$\frac{dn_{2\bar{A}}(\nu)}{dt}=\frac{-n_{2\bar{A}}(\nu)+p(\nu)g(\nu)N_{\bar{E}}}{T_d} \ , \tag{4}$$

where $N_{2\bar{A}}=\int_{-\infty}^{+\infty}n_{2\bar{A}}(\nu)d\nu$ is the total $2\bar{A}(^2E)$ population and $g(\nu)$ is the line shape normalized to unity. It is noted that Eq. (4) is applicable to both homogeneously

and inhomogeneously broadened transitions. In the present case, we have to discern the line shape of type-I ions, $g(\nu)$, from the line shape of type-II ions, $h(\nu)$. From fluorescence-line-narrowing experiments on Czochralsky-grown 700-at. ppm ruby, $g(\nu)$ was found to be adequately represented by a Voigt profile made up of a homogeneous part with a full width at half maximum of 240±15 MHz convoluted with an inhomogeneous profile with a full width at half maximum of 295±30 MHz.[11] The line shape $h(\nu)$ is not accurately known, but is likely to be of inhomogeneous nature and to be dependent on J. From an earlier analysis,[5,16] $h(\nu)$ was found to be substantially wider than $g(\nu)$, which is confirmed below.

A. Low phonon occupation

Upon combining the classification of the Cr^{3+} ions in type I and type II with the frequency-resolved treatment necessary to incorporate the line shapes, we have, for the rate equations at low phonon occupations $[p(\nu)\ll 1]$,

$$\frac{dn^{\mathrm{I}}_{2\bar{A}}(\nu)}{dt}=\frac{-n^{\mathrm{I}}_{2\bar{A}}(\nu)+p(\nu)g(\nu)N^{\mathrm{I}}_{\bar{E}}}{T_d}\ , \tag{5a}$$

$$\frac{dn^{\mathrm{II}}_{2\bar{A}}(\nu)}{dt}=\frac{-n^{\mathrm{II}}_{2\bar{A}}(\nu)+p(\nu)h(\nu)N^{\mathrm{II}}_{\bar{E}}}{T_d^{(n)}}+\frac{-n^{\mathrm{II}}_{2\bar{A}}(\nu)+p_{\mathrm{NR}}h(\nu)N^{\mathrm{II}}_{\bar{E}}}{T_d^{(f)}}\ , \tag{5b}$$

$$\rho\frac{dp(\nu)}{dt}=\frac{n^{\mathrm{I}}_{2\bar{A}}(\nu)-p(\nu)g(\nu)N^{\mathrm{I}}_{\bar{E}}}{T_d}+\frac{n^{\mathrm{II}}_{2\bar{A}}(\nu)-p(\nu)h(\nu)N^{\mathrm{II}}_{\bar{E}}}{T_d^{(n)}}\ , \tag{5c}$$

where ν denotes the frequency with respect to the center of the spin-nonflip transition. In Eqs. (5), the weak radiative decays of $\bar{E}(^2E)$ and $2\bar{A}(^2E)$ on a time scale of τ_R (≈3.4 ms) are neglected, and phonon-decay processes other than spectral wipeout by weakly coupled pairs are ignored. The direct spontaneous time constants in these equations are, as appropriate, the spin-nonflip and spin-flip times $T_d^{(n)}$ and $T_d^{(f)}$, and their parallel sum

$$T_d=(1/T_d^{(n)}+1/T_d^{(f)})^{-1}\ .$$

The occupation number of near-resonant (NR) phonons injected by the point contact, p_{NR}, is assumed to be maintained at a finite value during the phonon pulse and to be zero before and after the phonon pulse. Feeding of the resonant phonons by means of spectral wipein and their decay as a result of spectral wipeout are reflected in the spin-flip terms of Eq. (5b). Direct feeding of the phonon population bottlenecked by type-I Cr^{3+}, $p(\nu)$, is assumed to be absent since resonant phonons virtually do not penetrate the pumped zone.

The fastest rate occurring in Eqs. (5) is the rate $g(\nu)N^{\mathrm{I}}_{\bar{E}}/\rho T_d$ of spin-nonflip phonon absorption by type-I ions. For a typical $N^*\approx 10^{18}$ cm^{-3}, this rate is of order $10^2/T_d$ at resonance. On the time scale of interest here, therefore, $dp(\nu)/dt$ in Eq. (5c) can be ignored, so that to a very good approximation $p(\nu)$ is determined by the bottlenecking condition

$$p(\nu)=\frac{n^{\mathrm{I}}_{2\bar{A}}(\nu)/T_d+n^{\mathrm{II}}_{2\bar{A}}(\nu)/T_d^{(n)}}{g(\nu)N^{\mathrm{I}}_{\bar{E}}/T_d+h(\nu)N^{\mathrm{II}}_{\bar{E}}/T_d^{(n)}}\ . \tag{6}$$

To find the remaining two time constants of the combined spin-phonon system, we solve the homogeneous part of Eqs. (5a) and (5b) after substitution of $p(\nu)$ from Eq. (6), noting that $N^{\mathrm{I}}_{\bar{E}}$ and $N^{\mathrm{II}}_{\bar{E}}$ may be considered constants for $p(\nu)\ll 1$. Upon introducing the dimensionless quantity

$$\alpha(\nu)=g(\nu)N^{\mathrm{I}}_{\bar{E}}/h(\nu)N^{\mathrm{II}}_{\bar{E}}\ , \tag{7}$$

rigorous solution of the resulting eigenvalue problem then yields for the two time constants, the results T_d and

$$T_{\mathrm{eff}}(\nu)=\alpha(\nu)(T_d^{(f)}+T_d^{(n)})+T_d^{(f)}\ . \tag{8}$$

The associated eigenvectors indicate that the shorter time constant T_d (≈0.7 ns) is the time constant at which the populations $n^{\mathrm{I}}_{2\bar{A}}(\nu)$ and $n^{\mathrm{II}}_{2\bar{A}}(\nu)$ reach dynamical equilibrium via $p(\nu)$, and that the longer time constant $T_{\mathrm{eff}}(\nu)$ is associated with the decay of the combined $n^{\mathrm{I}}_{2\bar{A}}(\nu)-n^{\mathrm{II}}_{2\bar{A}}(\nu)$ system while maintaining the equilibrium ratio

$$n^{\mathrm{I}}_{2\bar{A}}(\nu)/n^{\mathrm{II}}_{2\bar{A}}(\nu)=\alpha(\nu)T_d^{(n)}/T_d\ . \tag{9}$$

On the time scale of the experiment, we are left with the single time constant $T_{\mathrm{eff}}(\nu)$.

For low $p(\nu)$ $[p(\nu)\ll 1]$, it is convenient to write $N^{\mathrm{I}}_{\bar{E}}=(1-f)N^*$ and $N^{\mathrm{II}}_{\bar{E}}=fN^*$, so that

$$\alpha(\nu)=(1-f)g(\nu)/fh(\nu)\ . \tag{10}$$

We further introduce the abbreviation $\phi(\nu)$ for the phonon feeding into $n^{\mathrm{II}}_{2\bar{A}}(\nu)$ during the point-contact pulse, or

$$\phi(\nu)=p_{\mathrm{NR}}fh(\nu)N^*/T_d^{(f)}\ . \tag{11}$$

For the quantity detected, the $2\bar{A}(^2E)$ population $N_{2\bar{A}}(t)=N^{\mathrm{I}}_{2\bar{A}}(t)+N^{\mathrm{II}}_{2\bar{A}}(t)$ integrated over the frequency, we then straightforwardly derive

$$N_{2\bar{A}}(t)=\begin{cases}\int_{-\infty}^{+\infty}\phi(\nu)T_{\mathrm{eff}}(\nu)\{1-\exp[-t/T_{\mathrm{eff}}(\nu)]\}d\nu & (t\le\tau_p) \quad (12a)\\ \int_{-\infty}^{+\infty}\phi(\nu)T_{\mathrm{eff}}(\nu)\{1-\exp[-\tau_p/T_{\mathrm{eff}}(\nu)]\}\exp[-(t-\tau_p)/T_{\mathrm{eff}}(\nu)]d\nu & (t>\tau_p)\ , \quad (12b)\end{cases}$$

where τ_p denotes the pulse duration. Equations (12a) and (12b) represent a non-single-exponential growth and decay of the frequency-integrated R_2 luminescence with time, respectively.

B. Elevated phonon occupation

At elevated phonon occupation [$p(\nu)$, $p_{\rm NR}\approx 1$], the rate equations are of considerable complexity because of the occurrence of stimulated emission and because the $\bar{E}(^2E)$ level becomes appreciably depopulated. Stimulated emission, for instance, leads to a broadening of the homogeneous line $g(\nu)$, which, in turn, invokes a coupling between phonons of various frequencies. A further complication is that at elevated $p(\nu)$ a substantial fraction of the Cr^{3+} in a pair reside in $2\bar{A}(^2E)$, modifying the distribution $h(\nu)$ of the type-II ions in $\bar{E}(^2E)$ [cf. Eq. (26) below].

Inclusive of stimulated emission, the rate equations read

$$\frac{dn^{\rm I}_{2\bar{A}}(\nu)}{dt}=\frac{-[p(\nu)+1]n^{\rm I}_{2\bar{A}}(\nu)+p(\nu)g_p(\nu)N^{\rm I}_{\bar{E}}}{T_d}\ , \tag{13a}$$

$$\frac{dn^{\rm II}_{2\bar{A}}(\nu)}{dt}=\frac{-[p(\nu)+1]n^{\rm II}_{2\bar{A}}(\nu)+p(\nu)h_p(\nu)N^{\rm II}_{\bar{E}}}{T_d^{(n)}}+\frac{-(p_{\rm NR}+1)n^{\rm II}_{2\bar{A}}(\nu)+p_{\rm NR}h_p(\nu)N^{\rm II}_{\bar{E}}}{T_d^{(f)}}\ , \tag{13b}$$

$$\rho\frac{dp(\nu)}{dt}=\frac{[p(\nu)+1]n^{\rm I}_{2\bar{A}}(\nu)-p(\nu)g_p(\nu)N^{\rm I}_{\bar{E}}}{T_d}+\frac{[p(\nu)+1]n^{\rm II}_{2\bar{A}}(\nu)-p(\nu)h_p(\nu)N^{\rm II}_{\bar{E}}}{T_d^{(n)}}\ , \tag{13c}$$

where the subscript p reminds one of the explicit $p(\nu)$ dependence of the line profiles. Obviously, Eqs. (13) defy analytical treatment, but considerations similar to those leading to the rigorous results for the case of vanishing $p(\nu)$ permit substantial simplifications to be made. Adding Eqs. (13a)–(13c), and again ignoring $dp(\nu)/dt$ in relation to the rates that correct for any departure of $p(\nu)$ on the right-hand side of Eq. (13c), we arrive at the quite general result

$$\frac{d[n^{\rm I}_{2\bar{A}}(\nu)+n^{\rm II}_{2\bar{A}}(\nu)]}{dt}=\frac{-(p_{\rm NR}+1)n^{\rm II}_{2\bar{A}}(\nu)+p_{\rm NR}h_p(\nu)N^{\rm II}_{\bar{E}}}{T_d^{(f)}}\ . \tag{14}$$

Detailed inspection of Eqs. (13) further reveals that, on the time scale of the experiment, i.e., $T_{\rm eff}(\nu)$, the combination of terms pertaining to type I and similarly the combination pertaining to type II each balance except for an amount $n^{\rm I}_{2\bar{A}}(\nu)/T_{\rm eff}(\nu)$. That is,

$$[p(\nu)+1]n^{\rm I}_{2\bar{A}}(\nu)=p(\nu)g_p(\nu)N^{\rm I}_{\bar{E}}\ , \tag{15a}$$

$$[p(\nu)+1]n^{\rm II}_{2\bar{A}}(\nu)=p(\nu)h_p(\nu)N^{\rm II}_{\bar{E}}\ . \tag{15b}$$

From this, we immediately see that the mutual equilibrium ratio of $n^{\rm I}_{2\bar{A}}(\nu)$ and $n^{\rm II}_{2\bar{A}}(\nu)$ is still given by Eq. (9) combined with Eq. (7) for $\alpha(\nu)$, but with the $p(\nu)$-dependent line shapes inserted. For the case of elevated $p(\nu)$, we have, accordingly,

$$\alpha_p(\nu)=g_p(\nu)N^{\rm I}_{\bar{E}}/h_p(\nu)N^{\rm II}_{\bar{E}}\ , \tag{16}$$

$$n^{\rm I}_{2\bar{A}}(\nu)/n^{\rm II}_{2\bar{A}}(\nu)=\alpha_p(\nu)T_d^{(n)}/T_d\ . \tag{17}$$

A more precise and detailed calculation shows that Eq. (17) holds apart from corrections of order

$$\alpha_p(\nu)T_d p(\nu)/T_{\rm eff}(\nu)[p(\nu)+1]\ ,$$

which amount to 5% at the highest $p(\nu)$. Using Eq. (17), we may rewrite Eq. (14) as

$$\left[\alpha_p(\nu)\frac{T_d^{(n)}}{T_d}+1\right]\frac{dn^{\rm I}_{2\bar{A}}(\nu)}{dt}=-\frac{(p_{\rm NR}+1)n^{\rm I}_{2\bar{A}}(\nu)}{T_d^{(f)}}+\alpha_p(\nu)\frac{T_d^{(n)}}{T_d}\phi_p(\nu)\ . \tag{18}$$

A similar expression may be derived for $n^{\rm II}_{2\bar{A}}(\nu)$. To extract $T_{\rm eff}$ from Eq. (18), we ignore, for the moment, the fact that it constitutes a non-single-exponential behavior because $\alpha_p(\nu)$ and $\phi_p(\nu)$ implicitly depend on time through the phonon occupations $p(\nu)$ at all frequencies. Upon realizing that

$$h_p(\nu)N^{\rm II}_{\bar{E}}+n^{\rm II}_{2\bar{A}}(\nu)=\text{const}$$

[cf Eq. (26) below], we further separate out a term $-p_{\rm NR}n^{\rm II}_{2\bar{A}}(\nu)/T_d^{(f)}$ from the high-p generalization of the phonon feeding

$$\phi_p(\nu)=p_{\rm NR}h_p(\nu)N^{\rm II}_{\bar{E}}/T_d^{(f)}\ , \tag{19}$$

and convert $n^{\rm II}_{2\bar{A}}(\nu)$ in this term to $n^{\rm I}_{2\bar{A}}(\nu)$ with the help of Eq. (17). We then find for the time constant of $n^{\rm I}_{2\bar{A}}(\nu)$ the final result

$$T_{\rm eff}(\nu)=\frac{\alpha_p(\nu)(T_d^{(f)}+T_d^{(n)})+T_d^{(f)}}{2p_{\rm NR}+1}\ , \tag{20}$$

which, quite naturally, amounts to a speeding up by a factor of $2p_{\rm NR}+1$ relative to the low-p case [cf. Eq. (8)].

An alternative, but convenient, way of incorporating both the phonon feeding and removal is to rewrite $g_p(\nu)N^{\rm I}_{\bar{E}}$ in terms of $n^{\rm I}_{2\bar{A}}(\nu)$ through the approximate expression Eq. (15a). We then have

$$dn^{\rm I}_{2\bar{A}}(\nu)/dt=-n^{\rm I}_{2\bar{A}}(\nu)/\tilde{T}_{\rm eff}(\nu) \tag{21}$$

with, apart from corrections of order $T_d^{(n)}/T_d^{(f)}\sim 10\%$,

$$\tilde{T}_{\rm eff}(\nu)=\frac{\alpha_p(\nu)(T_d^{(f)}+T_d^{(n)})+T_d^{(f)}}{1-p_{\rm NR}/p(\nu)}\ . \tag{22}$$

Note that this way of writing the development of $n^{\rm I}_{2\bar{A}}(\nu)$ does not imply that $n^{\rm I}_{2\bar{A}}(\nu)$ strives to zero. Rather, $\tilde{T}_{\rm eff}(\nu)$ is a net instantaneous time constant inclusive of the feeding. It increases with increasing $p(\nu)$ during the

pulse, such that the increase of $p(\nu)$ slows down when $p(\nu)$ approaches $p_{\rm NR}$. For $p_{\rm NR}=0$, of course, $\bar{T}_{\rm eff}(\nu)=T_{\rm eff}(\nu)$.

Up to this point, we have treated $\alpha_p(\nu)$ as a constant, whereas it, in fact, depends on $p(\nu)$. The dependence is accommodated in the time constant at any moment, which we have anticipated in Eqs. (20) and (22). Of the quantities occurring in $\alpha_p(\nu)$, the line shape $g_p(\nu)$, which is of a predominantly homogeneous nature, is represented by a Lorentzian, but with a width larger than that of $g(\nu)$ due to accelerated dephasing invoked by stimulated processes connecting $\bar{E}(^2E)$ and $2\bar{A}(^2E)$. Therefore,

$$g_p(\nu)=\frac{2\pi}{\Gamma(\bar{p})}\frac{\frac{1}{4}\Gamma^2(\bar{p})}{\frac{1}{4}\Gamma^2(\bar{p})+\nu^2}\ , \tag{23}$$

in which

$$\Gamma(\bar{p})=(2\bar{p}+1)\Gamma_0\ . \tag{24}$$

Here, Γ_0 is the low-temperature full line width at half maximum, while $\bar{p}$, defined by

$$\bar{p}=\int_{-\infty}^{+\infty} g_p(\nu)p(\nu)d\nu\ , \tag{25}$$

represents the appropriate weighted sum of $p(\nu)$ over the homogeneous line. With regard to the line shape $h_p(\nu)$, which, as already noted, is of inhomogeneous nature, it is related to the distribution $h^*(\nu)$ of the total excited-state population by

$$n^{\rm II}_{2\bar{A}}(\nu)+h_p(\nu)N^{\rm II}_{\bar{E}}=h^*(\nu)fN^*\ , \tag{26}$$

which, by use of the equilibrium condition Eq. (15b), leads to

$$\frac{2p(\nu)+1}{p(\nu)+1}h_p(\nu)N^{\rm II}_E=h^*(\nu)fN^*\ . \tag{27}$$

A similar dependence, but integrated over ν, holds for the homogeneous line shape $g_p(\nu)$. That is,

$$N^I_{\bar{E}}\int_{-\infty}^{+\infty}\frac{2p(\nu)+1}{p(\nu)+1}g_p(\nu)d\nu=(1-f)N^*\ . \tag{28}$$

Under the condition of a flat photon spectrum, therefore,

$$\alpha_p(\nu)=g_p(\nu)(1-f)/h^*(\nu)f\ . \tag{29}$$

IV. RESULTS AND DISCUSSION

The previous section has shown that the line shape of the phonon transition is directly reflected in the relaxation of the coupled spin-phonon system. As a matter of fact, $T_{\rm eff}(\nu)$ is longest in the line center, becoming shorter towards the wings, as expressed by Eqs. (8) and (20). As a result, the temporal development of the quantity observed, viz., the $2\bar{A}(^2E)$ population integrated over all frequencies, will be nonsingle exponential [cf. Eqs. (12)].

A. Low phonon occupation

We first consider the case of weak phonon feeding by the point contact, resulting in low phonon occupations. A selection of time-resolved recordings of the frequency-integrated R_2 luminescent intensity, which is proportional to the $2\bar{A}(^2E)$ population, is shown in Fig. 3. Each trace reflects an initial growth of the integrated $2\bar{A}(^2E)$ population $N_{2\bar{A}}(t)$ for the duration of the pulse, followed by a decay after removal of the phonon feeding. Thermal phonons are essentially absent at the relevant temperature (1.5 K). The traces presented are taken from a series with different durations τ_p of the electrical pulse, but identical power dissipation in the contact (0.1 W). The advantage of varying the pulse duration is that, because at shorter τ_p the emphasis shifts towards frequencies with shorter $T_{\rm eff}(\nu)$ [cf. Eq. (12b)], it allows one to probe different parts of the relaxation-time distribution. Inspection of the decays shows that they are markedly nonsingle exponential, particularly at the shorter τ_p. Further, the decays become slower for longer pulse durations.

To account for the traces of Fig. 3, we have simultaneously adjusted Eq. (12a) for the buildup and Eq. (12b) for the decay after substitution of Eq. (8) for $T_{\rm eff}(\nu)$ and Eq. (11) for $\phi(\nu)$. In $T_{\rm eff}(\nu)$, in turn, $\alpha(\nu)$ from Eq. (7) was in-

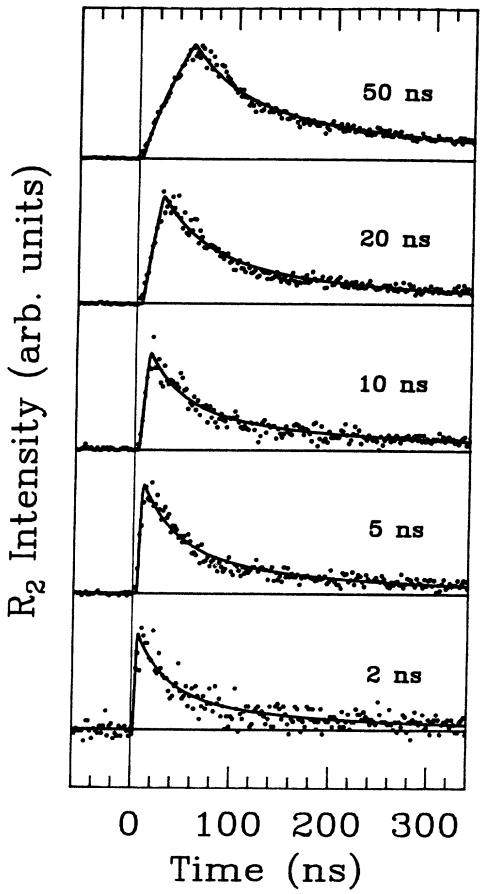

FIG. 3. The integrated R_2 intensity vs time for various durations of the phonon pulse. Data apply to $N^*\sim 2\times 10^{18}$ cm^{-3} and $L=50$ μm. The power dissipated in the point contact is approximately 0.1 W. The solid curves represent fits of Eqs. (12) with a Lorentzian $g(\nu)$. The traces are mutually not to scale.

serted. The line shape $h(\nu)$ occurring in the expressions for $\alpha(\nu)$ and $\phi(\nu)$ was taken as flat on the grounds that $h(\nu)$ is much broader than $g(\nu)$, and thus virtually constant in the central range of frequencies carrying most of the weight. In this connection, it is also noted that the combination $fh(\nu)$ drops out of the product $\phi(\nu)T_{\text{eff}}(\nu)$ occurring in the integrands of Eqs. (12). Further, $T_d^{(n)} \approx 0.7$ ns and $T_d^{(f)} \approx 12$ ns. In summing up, therefore, we are left with $(1-f)/fh(0)$ as fitting the parameter, apart from a trivial scaling factor η relating $N_{2\bar{A}}(t)$ to the R_2 intensity.

Fits to the five traces in Fig. 3 have been accomplished for $g(\nu)$ having the shape of a Lorentzian to a power γ, with γ an additional fitting parameter, and $g(\nu)$ having a Voigt profile as derived from FLN studies.[11] Irrespective of the choice of $g(\nu)$, the fits are not significantly different between the five traces with regard to the result $(1-f)/fh(0)$. In another fit, comprising all five traces simultaneously, $(1-f)/fh(0)$ and the five η's were varied, yielding essentially the same results. In particular, the fits for the Lorentzian, represented in Fig. 3 by the solid curves, excellently track the data over the full time span. For the Lorentzian, the output values of the fitting parameters are

$$(1-f)/fh(0)=(50\pm5)\Gamma_0$$

and $\gamma=1.02\pm0.05$; for the Voigt profile,

$$(1-f)/fh(0)=(40\pm7)\Gamma_0 .$$

With respect to the overall prefactor, i.e., the instrumental factor η times the phonon feeding $\phi(\nu)$, it turned out to be the same for all fits within a factor of 2. This is, in fact, quite satisfactory in view of the uncertainties in p_{NR} and η from trace to trace. Reasonably accurate estimates can be deduced for the quantity f from the wipeout condition, Eq. (2), and the expression for the mean free path, Eq. (3). For $N^* \approx 2\times10^{18}$ cm^{-3} in 700-at. ppm ruby and the relevant $L \sim 50$ μm, we then arrive at $f \sim 0.13$ with the help of the expressions given in Ref. 5. Accordingly, the fits indicate that $h(\nu)$ has a width of order $8\Gamma_0$, which is consistent with what has been inferred from the detailed analysis of the relaxation time versus N^*L in Ref. 5, and, more recently, from Monte Carlo simulations of the itinerary of imprisoned phonons in the optically excited zone.[10]

B. Elevated phonon occupation

We now turn to the measurements at high phonon occupation. In Fig. 4, the total $2\bar{A}(^2E)$ population, as reflected in the intensity of the R_2 luminescence, is presented as a function of time for various values of the electrical power applied to the point contact. All recordings refer to $N^* \sim 10^{19}$ cm^{-3}, not far from the maximum attainable N^* in 700-at. ppm ruby, and $L=200$ μm. The excitation pulse was taken to last for 2.9 μs. This duration is significantly longer than all time scales involved, but is imperative if high phonon occupations are to be reached at a power below breakdown of the point contact. It is noted in this context that the experiments have been repeated with a pulse duration of 1.0 μs. This yielded essentially the same conclusions, although for a given N^*L complete saturation of the R_2 intensity was not attained at lower electrical power. The trace at 0.03-W electrical power may still be considered to refer to the low-p case, even at the long pulse durations used. This was confirmed by a series of traces, not shown here, for pulses down to 10^{-4} W, which turned out to be indistinguishable from the 0.03-W case except for a trivial scaling of the overall amplitude. The growth and the decay at 0.03 W are nonsingle exponential, much like the traces for low p presented in Fig. 3. They can be accounted for by Eqs. (12). For 0.03 W, we then find

$$(1-f)/fh(0)=(180\pm20)\Gamma_0 .$$

This result is consistent with the corresponding result deduced from Fig. 3 if the reduction of f associated with the increase of N^*L is taken into account (cf. Ref. 5).

Having discussed the lowest-p trace, we consider the changes that occur in the time traces upon increasing the point-contact power. In Fig. 4, it is clearly seen that both the rise and the fall of the R_2 luminescence become

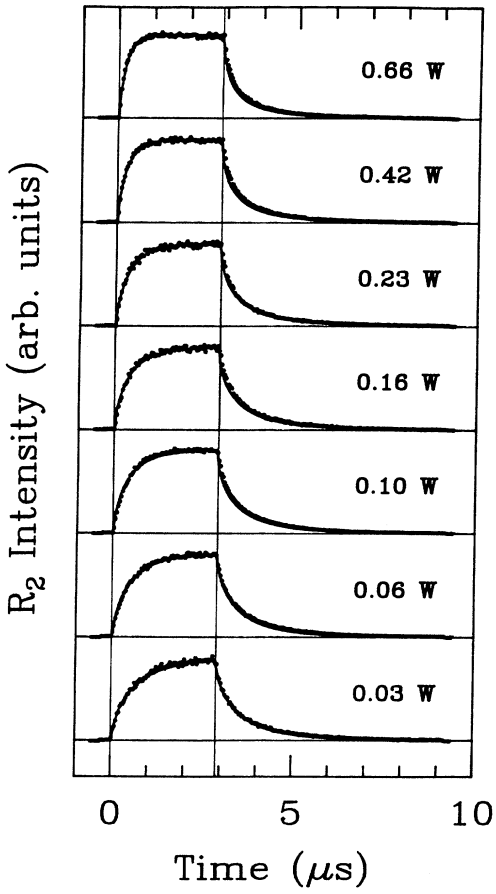

FIG. 4. The R_2 luminescent intensity (solid circles) and the calculated $N_{2\bar{A}}$ (solid curves) vs time for various dissipations in the point contact. The traces are scaled individually. $N^* \sim 10^{19}$ cm^{-3} and $L \sim 200$ μm.

markedly faster in comparison with the lowest-p trace. Closer inspection, however, reveals that the rise is more profoundly affected than the decay, which indicates that the speeding up is caused at least in part by the externally supplied phonon occupation p_{NR}. Closer inspection further makes it clear that the traces have become more nonsingle exponential, in the sense that the amplitudes of the faster components have gained with respect to the slower ones.

Before carrying out the full quantitative analysis, it is of interest to point out that the effects on the time constants during rise and decay are indeed contained in the theory developed above. To clarify this, we refer to Eq. (20) for $T_{\mathrm{eff}}(\nu)$. First, Eq. (20) predicts an overall speeding up by a factor $2p_{\mathrm{NR}}+1$ related to stimulated spin-flip processes connecting near-resonant phonons with type-II spins. Obviously, this factor does not influence the decay following the pulse, where p_{NR} has dropped to zero, nor does it add to the nonsingle exponentiality. Second, the frequency dependence of the quantity $\alpha_p(\nu)$ occurring in Eq. (20) notably broadens during the rise, with a corresponding reduction of the amplitude, if the resonant phonon occupation becomes of order unity. Note here that, as far as its frequency dependence is concerned, $\alpha_p(\nu)$ is almost entirely governed by the type-I line shape $g_p(\nu)$, so that it is, in effect, broadened and reduced in amplitude by a factor $2\bar{p}+1$ [cf. Fig. 5, and Eqs. (23) and (24)]. Conversely, $\alpha_p(\nu)$ sharpens up to its low-p limit $\alpha(\nu)$ during the decay. In terms of time constants, the variation of $\alpha_p(\nu)$ with the phonon occupation causes a shift of the weight from slower towards faster $T_{\mathrm{eff}}(\nu)$ during the rise, and vice versa during the decay, which enhances the nonsingle exponentiality. In summary, therefore, the rise speeds up with increasing electrical power because of the combined effect of p_{NR} and the broadening of the phonon transition, while the decay accelerates by the broadening alone. A further characteristic of the theory is that the rise and decay do not depend on N^* and L except for a scaling via the fraction f of type-II centers [cf. Eq. (29)]. To confirm the latter point in some detail, R_2 traces such as in Fig. 4 have also been taken for $N^*=3\times10^{18}$, 10^{18}, and 3×10^{17} cm^{-3} under otherwise the same conditions.

In the quantitative analysis, the development of $n^{\mathrm{I}}_{2\bar{A}}(\nu)$ with time has been evaluated by numerical integration of Eq. (18), or its alternative Eq. (21), for a series of p_{NR} values. To this end, the frequency range is divided up into 64 intervals of identical width, covering $3\Gamma_0$ on either side. The starting values of all $p(\nu)$ at the beginning of the pulse, where $\Gamma(\bar{p})$ still equals Γ_0, are set according to a temperature of 1.5 K. The initial $2\bar{A}(^2E)$ populations $n^{\mathrm{I}}_{2\bar{A}}(\nu)$ and $n^{\mathrm{II}}_{2\bar{A}}(\nu)$ are subsequently derived by the use of the dynamical equilibrium conditions Eqs. (15a) and (15b). The product N^*L is fixed at the relevant 2×10^{17} cm^{-2}, resulting in $f=0.05$. Next, p_{NR} is switched on for a time $\tau_p=2.9$ μs, as in the experiments. Each step of the numerical integration then consists of, given the current $g_p(\nu)$, calculating $n^{\mathrm{I}}_{2\bar{A}}(\nu)$ for each of the 64 ν after a sufficiently small time lapse, computing the associated $p(\nu)$ by use of Eq. (15a), determining a new $\bar{p}$ by averaging the new $p(\nu)$ according to Eq. (25), and finally evaluating a new set of $g_p(\nu)$ from Eq. (23). For a comparison with the measured time traces of the R_2 luminescence, the frequency- and time-dependent sum spectrum $n_{2\bar{A}}(\nu)=n^{\mathrm{I}}_{2\bar{A}}(\nu)+n^{\mathrm{II}}_{2\bar{A}}(\nu)$ is subsequently calculated from $n^{\mathrm{I}}_{2\bar{A}}(\nu)$ by use of Eq. (29). For $\rho_{\mathrm{NR}}=0.66$, as a case in point, the temporal developments of $g_p(\nu)$ and $n_{2\bar{A}}(\nu)$ are shown in Fig. 5, where the range of frequencies has been extended to $10\Gamma_0$. The quantity $n_{2\bar{A}}(\nu)$ is finally integrated over frequency to obtain $N_{2\bar{A}}(t)$.

The results of the calculations have been fitted to each of the experimental traces in Fig. 4, with p_{NR} and a proportionality factor η, relating $N_{2\bar{A}}(t)$ to the R_2 intensity, as adjustable parameters. The fitted $N_{2\bar{A}}(t)$ are entered in Fig. 4 as the solid curves, and seen to faithfully reproduce the experimental R_2 traces. As it turns out, phonon occupations p_{NR} as high as 0.66 have been attained. Quite remarkably, the resultant p_{NR} depend, within errors, linearly on the electrical power up to the highest p_{NR}, as is shown in Fig. 6. The origin of this linearity is

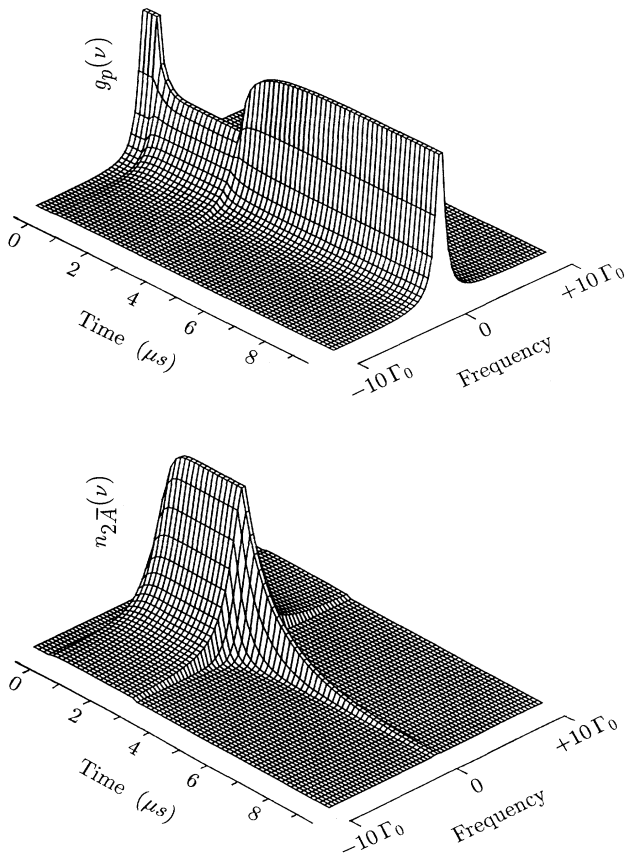

FIG. 5. The quantities $g_p(\nu)$ and $n_{2\bar{A}}(\nu)$ vs time for $p_{\mathrm{NR}}=0.66$. The pulse duration is 2.9 μs, and $N^*L=2\times10^{17}$ cm^{-2}.

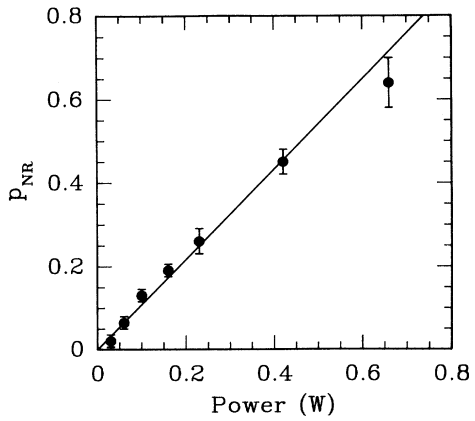

FIG. 6. The near-resonant phonon occupation p_{NR} supplied by the point contact vs the electrical power. The solid points are deduced from the fits of $N_{2\bar{A}}(t)$ to the experimental data of Fig. 4. The solid line corresponds to a linear dependence.

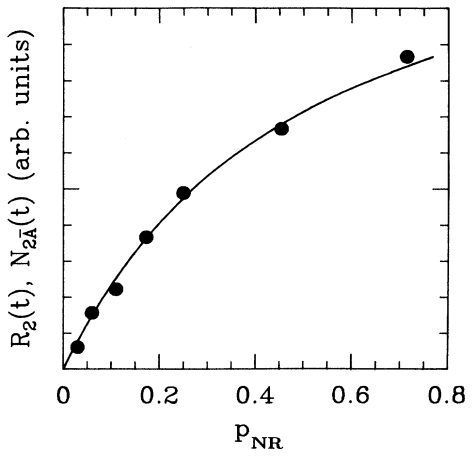

FIG. 7. Comparison of the experimental R_2 intensities (solid circles) and the theoretical $N_{2\bar{A}}(t)$ (solid curve) vs p_{NR} at the end of the external phonon supply ($t=\tau_p$).

to be found in the fact that the extent of the "hot spot," i.e., the regime of thermalization of phonons below the point contact, is determined by the phonon mean free path. As a consequence, an increase in the electrical power results in a large hot-spot radius, but not in a marked variation of the surface temperature of the spot. In ruby, the hot spot has a surface temperature of approximately 60 K, and, at 1-W power, a radius of about 10 μm.[18]

The traces of Fig. 4 have been measured with sufficient care to permit a comparison of the absolute experimental R_2 luminescent intensities with theoretical $N_{2\bar{A}}(t)$. In the fits this is expressed by the fact that the factors η coincide among the various traces. In Fig. 7, the R_2 intensities at the end of the pulse are plotted, in arbitrary units, versus p_{NR}(data entries) and compared with $N_{2\bar{A}}(\tau_p)$ (solid line). Note the flattening out with increasing p_{NR}, signifying that a substantial fraction of the Cr^{3+} population resides in $2\bar{A}(^2E)$. The agreement once more illustrates that the theory gives an excellent reproduction of the experimental data.

To conclude this section, we briefly discuss to what extent the fitted curves are dependent on the mechanisms of phonon feeding and phonon loss. As examples, we consider direct feeding of the resonant phonons by the outside source and local linear phonon loss of the form $-p(\nu)/\tau$, with τ a time constant, instead of feeding and loss by mediation of Raman shifting. Treating resonant feeding requires solving for the phonon populations at various frequencies in both time and space because the mean free path of resonant phonons is of the order of a μm or less. This problem has been examined earlier by use of Monte Carlo simulations,[10] which showed that resonant phonons do not significantly penetrate into the excited zone, i.e., they do not provide sufficient feeding throughout the excited volume. With regard to linear phonon loss, appropriate rate equations of the form of Eqs. (13) yield an effective relaxation time $T'_{\rm eff}(\nu)=\alpha'_p(\nu)\tau/[2p(\nu)+1]$, with $\alpha'_p(\nu)=g_p(\nu)N_{\bar{E}}/\rho$. For $p(\nu)\ll 1$, this $T'_{\rm eff}(\nu)$ does not lead to a frequency dependence different from Eq. (8). For $p(\nu)\gtrsim 1$, the frequency dependence of $T'_{\rm eff}(\nu)$ is more pronounced than the frequency dependence of $T_{\rm eff}(\nu)$ resulting from Raman shifting [Eq. (20)] because $p(\nu)$ depends on the frequency. In comparison with $T_{\rm eff}(\nu)$, $T'_{\rm eff}(\nu)$ furthermore depends on the time through the actual $p(\nu)$ rather than the imposed p_{NR}. These modifications would clearly yield fits to the data of the R_2 intensity versus time which are of a quality inferior to those in Fig. 4. The integration of the decay over the frequency, which is inherent to the present experiments [cf. Eqs (12)], however, renders the differences marginal.

V. CONCLUSIONS

The trapping of 29-cm^{-1} phonons in ruby at 1.5 K has been studied up to substantial nonequilibrium phonon occupation numbers ($p\sim 1$). The phonons have been generated with a metallic whisker-film point contact. Due to the small size of the point contact, ns time resolution was achieved, and intense phonon pulses could be injected even with moderate absolute powers. In experiments at low phonon occupations, employing short phonon pulses of variable duration, a marked non-single-exponential growth and decay of the trapped phonon population has been observed. A detailed analytical description has been developed on the basis of rate equations with explicit allowance for the line shape of the $\bar{E}(^2E)-2\bar{A}(^2E)$ phonon transition as well as for the loss and feeding of resonant phonons by mediation of weakly exchange-coupled Cr^{3+} pairs. From this treatment, it is concluded that the line shape profoundly affects the phonon trapping. Experiments at higher phonon occupations over a longer

duration showed an overall acceleration of the decay due to the occurrence of stimulated processes. Moreover, an increased nonsingle exponentiality has been found, which is caused by a dynamical broadening of the $\overline{E}(^2E)-2\overline{A}(^2E)$ transition by stimulated processes involving resonant phonons. The point contact appeared to inject near-resonant phonons up to occupations of 0.7 averaged over the detection volume.

ACKNOWLEDGMENTS

The authors thank C. R. de Kok for his invaluable and skillful technical assistance. The work was financially supported by the Netherlands Foundation "Fundamenteel Onderzoek der Materie" (FOM) and the "Nederlandse Organisatie voor Wetenschappelijk Onderzoek" (NWO).

[1]S. Geschwind, G. E. Devlin, R. L. Cohen, and S. R. Chinn, Phys. Rev. **137**, A1087 (1965).

[2]K. F. Renk and J. Deisenhofer, Phys. Rev. Lett. **26**, 764 (1971).

[3]J. I. Dijkhuis and H. W. de Wijn, Phys. Rev. B **20**, 1844 (1979); Solid State Commun. **31**, 39 (1979).

[4]R. S. Metlzer, J. E. Rives, and W. C. Egbert, Phys. Rev. B **25**, 3026 (1982).

[5]R. J. G. Goossens, J. I. Dijkhuis, and H. W. de Wijn, Phys. Rev. B **32**, 7065 (1985).

[6]S. A. Basun, A. A. Kaplyanskii, and S. P. Feofilov, Fiz. Tverd. Tela **28**, 3616 (1986) [Sov. Phys. Solid State **22**, 2055 (1986)].

[7]J. A. Giordmaine and F. R. Nash, Phys. Rev. **138**, A1510 (1965).

[8]S. A. Basun, A. A. Kaplyanskii, S. P. Feofilov, and V. L. Shektman, Fiz. Tverd. Tela **25**, 2731 (1983) [Sov. Phys. Solid State **25**, 1570 (1983)].

[9]K. F. Renk, in *Phonon Scattering in Condensed Matter,* edited by W. Eisenmenger, K. Lassmann, and S. Döttinger (Springer-Verlag, Berlin, 1984), p. 10.

[10]M. J. van Dort, J. I. Dijkhuis, and H. W. de Wijn, Phys. Rev. B **41**, 8657 (1990).

[11]M. J. van Dort, M. H. F. Overwijk, J. I. Dijkhuis, and H. W. de Wijn, Solid State Commun. **72**, 237 (1989).

[12]R. J. G. Goossens, J. I. Dijkhuis, and H. W. de Wijn, A. G. M. Jansen, and P. Wyder, Physica B **127**, 422 (1984).

[13]C. H. Anderson and E. S. Sabisky, Appl. Phys. Lett. **13**, 214 (1968).

[14]M. H. F. Overwijk, P. J. Rump, J. I. Dijkhuis, and H. W. de Wijn (unpublished).

[15]K. L. Chopra, *Thin Film Phenomena* (McGraw-Hill, New York, 1969), p. 318.

[16]S. Majetich, R. S. Meltzer, and J. E. Rives, Phys. Rev. B **38**, 11 075 (1988).

[17]K. F. Renk, in *Nonequilibrium Phonons in Nonmetallic Crystals,* edited by W. Eisenmenger and A. A. Kaplyanskii (Elsevier, Amsterdam, 1986), p. 317.

[18]K. Z. Troost, M. J. van Dort, J. I. Dijkhuis, and H. W. de Wijn, Phys. Rev. B **43**, 98 (1991).